








Cite this: *Nanoscale Horiz.*, 2025, 10, 1674

Received 28th January 2025,
Accepted 19th May 2025

DOI: 10.1039/d5nh00045a

rsc.li/nanoscale-horizons

Dot-blot immunoassay based on antibody-nanocluster biohybrids as tags for naked-eye detection†

Verónica Mora-Sanz, ^{*a} Laura Saa, ^b Valeri Pavlov, ^b
Aitziber L. Cortajarena, ^{bc} Bergoi Ibarlucea ^{*a} and Nerea Briz ^{*a}

Paper-based assays such as dot-blot show high promise to develop point-of-care testing devices fulfilling the ASSURED requirements suggested by the World Health Organization (affordable, sensitive, specific, user-friendly, rapid and robust, equipment-free, and deliverable). In this technique, natural enzymes are conventionally employed tags to provide bioreceptors such as antibodies with catalytic activity for quantitative assessment. Nonetheless, their inherent biomolecular limitations pose significant challenges, including cost and storage constraints. We propose an alternative conjugation for antibodies based on catalytic bimetallic nanoclusters and their integration in such simple colorimetric paper-based immunoassay. The nanoclusters are composed of gold and platinum and they are embedded in the structure of an anti-rabbit antibody, integrating in a single component the biorecognition and transduction elements required for biosensing. The detection is based on the catalytic properties of the NCs to oxidize an insoluble chromogenic substrate, generating a visible signal on the surface of the paper that can be further analysed for quantitative results. We demonstrate the detection of antibodies against the inflammation biomarker interleukin-6 with a limit of detection of 200 ng mL⁻¹. Experimental results reveal improvements in terms of stability compared to the natural enzyme horseradish peroxidase, retaining most of its activity after a storage equivalent to 6 months at 4 °C. Additionally, incorporating the NCs within the antibody structure instead of attaching them *via* a covalent bond provides an enhanced sensitivity of 69.7%. This assay could be transferred to other specific antibodies to detect and quantify other analytes of interest.

New concepts

We introduce a novel concept: secondary antibodies with bimetallic nanoclusters (NCs) integrated into their structure, serving as detection antibodies in paper-based immunoassays for naked-eye detection. The NCs, composed of gold and platinum, endow the antibodies with intrinsic catalytic activity, enabling the oxidation of chromogenic substrates without requiring additional crosslinking steps or external conjugation processes. Unlike existing approaches in the literature that rely on nanomaterials conjugated *via* covalent bonds, this method incorporates the NCs directly into the antibody structure, streamlining the synthesis process and enhancing performance. This concept also addresses key limitations of conventional methods using natural enzymes like horseradish peroxidase (HRP), which suffer from stability and storage constraints. Experimental results demonstrate that the NC-integrated antibodies retain most of their catalytic activity after storage equivalent to six months at 4 °C, significantly outperforming HRP. Moreover, embedding NCs directly into the antibody structure enhances detection sensitivity by 69.7% compared to covalent attachment methods. This work brings new insights into nanoscience and nanotechnology by demonstrating a universal strategy for integrating nanomaterials into biomolecules, paving the way for highly stable, sensitive, and scalable biosensing platforms. The approach can be extended to other antibodies for detecting and quantifying various analytes of interest.

1. Introduction

Dot-blot assays have received significant consideration in diagnosis due to rapid analysis, selectivity, low cost and ease of use, making them suitable for the point-of-care (PoC) test.¹ The advantage of visible colorimetric detection over fluorescence in dot-blot assays is the lack of specialized equipment needed for excitation and signal measurement in semiquantitative assays.¹ The results from colorimetric assays are also easier to interpret visually without complex data processing. Furthermore, in fluorescent dot blots, the most

^a TECNALIA, Basque Research and Technology Alliance (BRTA), Mikeletegi Pasealekua 2, 20009, Donostia-San Sebastian, Spain. E-mail: veronica.mora@tecnalia.com, bergoi.ibarlucea@tecnalia.com, nerea.briz@tecnalia.com

^b Center for Cooperative Research in Biomaterials (CIC biomaGUNE), Basque Research and Technology Alliance (BRTA), Paseo de Miramón 194, 20014, Donostia-San Sebastián, Spain

^c Ikerbasque, Basque Foundation for Science, 48009, Bilbao, Spain

† Electronic supplementary information (ESI) available. See DOI: <https://doi.org/10.1039/d5nh00045a>

commonly used tags are organic fluorophores and quantum dots (QDs). However, organic fluorophores have very small Stokes shifts and are susceptible to photobleaching,² whereas some QDs (CdS, CdTe, or CdSe) are toxic to the environment and biological systems, limiting their use.³ Therefore, colorimetric dot blots are preferable in many applications, especially when access to sophisticated equipment is limited or when simplicity and speed are essential,⁴ which are expected pre-requisites for paper-based assays.

Enzymes are usually conjugated to detection antibodies for signal amplification in conventional colorimetric dot-blot assays. One of the most employed enzymes is horseradish peroxidase (HRP). Different insoluble substrates can be used with HRP in dot-blot assays such as 3,3',5,5'-tetramethylbenzidine (TMB) in the presence of hydrogen peroxide (H₂O₂). Natural enzymes have intrinsic limitations such as high cost for preparation and purification, low stability, difficulty in storage, sensitivity of catalytic activity to environmental conditions and difficulties in recycling and storage.⁵ These disadvantages have stimulated the emergence and development of enzyme mimics also called artificial enzymes.⁶ Different materials can act as artificial enzymes such as cyclodextrins, cyclophanes, palladium-based artificial enzymes, hemin-based organic phase artificial enzymes, vitamin B12 and ethyleneimine polyethyleneimine.⁷ Among them the most promising materials are nanozymes, since the discovery of peroxidase-like activity of Fe₃O₄ in 2007.⁸ Nanozymes are materials in the nanoscale that can mimic the behaviour of an enzyme.⁹ In comparison with natural enzymes, nanozymes have a stable structure, adjustable activity and diverse functions, making them potential substitutes for natural enzymes in many fields,¹⁰ from healthcare¹¹ to environmental applications.¹² The peroxidase-like activity of some nanozymes has led to the successful design of nanozyme-based biosensors for the detection of ions,¹³ small molecules,¹⁴ nucleic acids¹⁵ or proteins.¹⁶

The literature reports examples of paper-based immunoassays employing NPs with peroxidase-like activity. For example, platinum–palladium (Pt/Pd) nanoparticles were applied as signal amplifiers in dual-lateral flow immunoassays (LFIA) and integrated with a smartphone-based device for simultaneous detection of *Salmonella enteritidis* and *Escherichia coli*.¹⁷ Another example is the use of Fe₃O₄ magnetic NPs, as a nanozyme probe for the development of an immunochromatographic strip which detects the glycoprotein of Ebola virus as low as 1 ng mL⁻¹, which is 100 times more sensitive than the standard strip.¹⁸ Recently another immunochromatographic assay was described based on polydopamine-mediated magnetic (Fe₃O₄) bimetallic (Pd/Pt) NPs for the detection of human chorionic gonadotropin in human blood serum and *E. coli* in milk samples.¹⁹

Alternatively, nanoclusters (NCs) fill the gap between NPs and single atoms and are composed of few to roughly several hundred atoms, with sizes from 0.2 to 3 nm.^{20,21} NCs are characterized by sizes comparable to the Fermi wavelength of electrons and exhibit molecule-like properties, such as catalytic activity.²² Due to their unique properties, NCs find important applications in biodetection.²³ NCs have a higher surface/volume ratio than bigger NPs and higher catalytic activity in comparison with other nanomaterials of the same mass. As the

diameter of the particle decreases, the fraction of exposed surface sites increases, resulting in an improvement in the catalytic activity.²⁴

Template-based NC synthesis methods employ stabilizing agents to guide and control particle formation. Among these, the use of biomolecules as scaffolds results in biohybrid structures. Specifically, when antibodies are employed as scaffolds, the bioreceptor and the transducing element are integrated in a single component. Several proteins have been used as scaffolds for the synthesis of metallic NCs, such as bovine serum albumin (BSA),^{25–27} pepsin,^{28,29} trypsin,²⁹ lysozyme,²⁹ papain³⁰ or human serum albumin (HSA).³¹ Proteins have natural metal coordination groups in their composition, like sulfhydryl groups, hydroxyl groups, carboxyl groups, amines and reducing amino acid residues, for example, cysteine, tryptophan, and tyrosine. The coordination chemistry between the metal atoms in the core surface of the NCs and the biomolecules, along with the large steric hindrance and reducing properties makes possible the controllable synthesis of NCs. Engineered protein scaffolds further enhance the ability to systematically and precisely synthesize nanoclusters with specific properties, revealing the influence of the protein component on the final properties of the scaffold.^{32–36}

While many synthesis methods are usually performed under denaturing conditions (pH, temperature...) and in most of the cases, the structure of the protein is altered, and it loses its biological properties. Previously reported synthesis methods^{35–38} allow the functionality of the antibody during the incorporation of the NCs into its structure. The protein conformation remains unchanged, preserving the affinity for the target analyte. Combining the peroxidase-like properties of Au/Pt NCs³⁹ and the specific antibody recognition enabled Au/Pt NCs–IgG to be employed as a probe integrating the sensing element and the transducer in dot-blot immunoassays.^{37,38}

In this work, we incorporate the advantageous approach of antibody-protected bimetallic NCs composed of gold and platinum (Au/Pt NCs–IgG) with peroxidase-like properties to a colorimetric dot-blot immunoassay (Fig. 1). A secondary polyclonal antibody (anti-rabbit IgG) was chosen as the NC host for the detection of rabbit anti-IL-6 IgGs. IL-6 is a relevant biomarker for inflammation and immune response, playing a crucial role in various diseases, including autoimmune disorders,⁴⁰ cancer,⁴¹ and infectious diseases.⁴²

Detecting anti-IL-6 antibodies based on this dot-blot assay represents a promising affordable tool for monitoring biological therapies to ensure their efficacy,⁴³ as well as for the diagnosis and prognosis of autoimmune and inflammatory diseases. Along with the analysis of the biosensing response, we perform a stability study to evaluate the performance of the biohybrid structures in the long term.

2. Experimental

2.1. Materials

Chloroauric acid (HAuCl₄), potassium tetrachloroplatinate (K₂PtCl₄), sodium borohydride (NaBH₄), polyclonal anti-rabbit

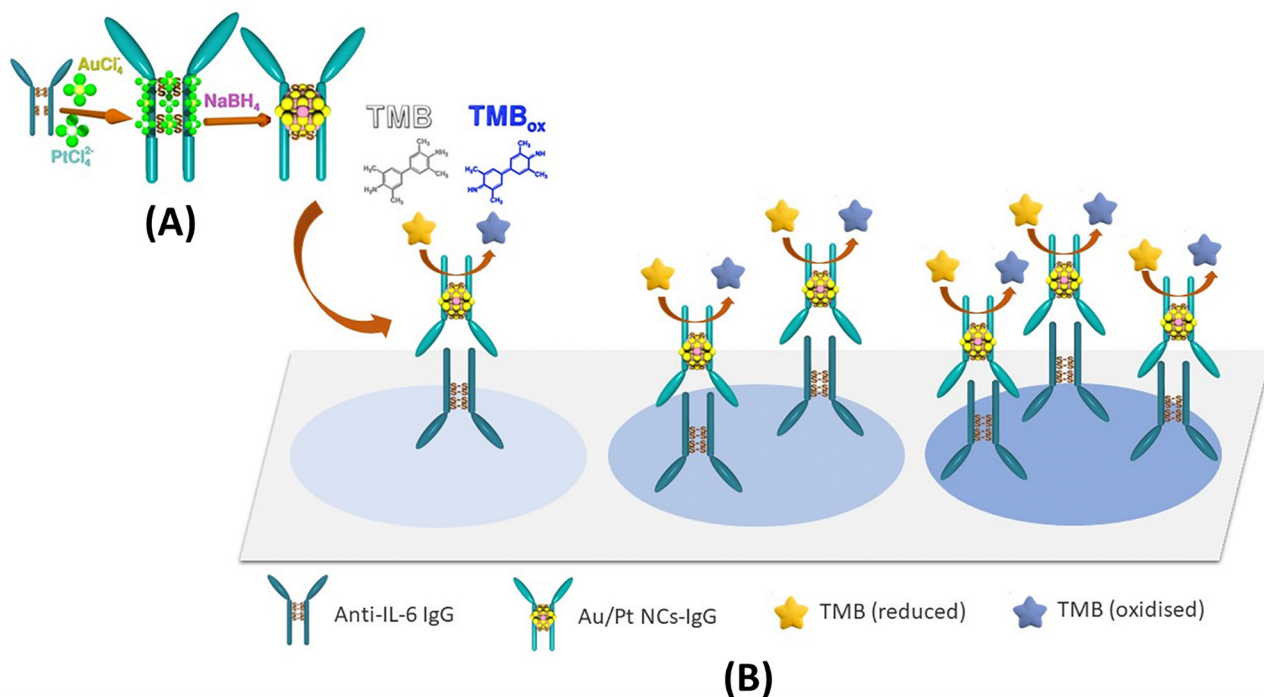


Fig. 1 (A) Scheme of the synthesis of Au/Pt NCs employing anti-rabbit IgG as a scaffold. (B) Paper-based immunoassay for IgG from rabbit quantification employing the peroxidase-like properties of Au/Pt NCs-IgG.

IgG (developed in goat), TMB, TMB liquid substrate system for membranes, phosphate-buffered saline (pH 7.4) (PBS), phosphate-buffered saline Tween[®]-20 (PBST), *N*-(3-dimethylaminopropyl)-*N'*-ethylcarbodiimide (EDC), 4-morpholineethanesulfonic acid (MES), casein blocking buffer, serum from human male AB plasma and other chemicals were purchased from Sigma-Aldrich. H_2O_2 was supplied by PanReac. Anti-IL-6 IgG from rabbits and *N*-hydroxysulfosuccinimide (sulfo-NHS) were purchased from Fisher Scientific. The nitrocellulose transfer membrane (0.22 μm) was obtained from Abcam.

2.2. Synthesis of Au/Pt NCs-IgG

The Au/Pt NCs embedded in the structure of IgG were synthesized based on a previously reported method³⁷ with slight changes. In this work, the synthesis was set up for the antibody of this study, polyclonal anti-rabbit IgG. Briefly, a solution of polyclonal anti-rabbit antibody (330 $\mu\text{g mL}^{-1}$) in PBS (pH 7.4) was mixed with HAuCl_4 (25 μM) and K_2PtCl_4 (200 μM) and incubated in the dark for 30 min. NaBH_4 (0.5 mM) was then added as a reducing agent, changing the mixture color from colorless to pale brown. The solution had a final volume of 300 μL and it was incubated for 1 h at room temperature (RT) and filtered using Amicon filters (30 kDa cutoff) at $10\,000 \times g$ for 15 min to separate free ions from the NCs.

2.3. Synthesis of IgG@Au/Pt NCs-bovine serum albumin bioconjugates

To prepare IgG@Au/Pt NCs-bovine serum albumin bioconjugates (IgG@Au/Pt NCs-BSA), anti-rabbit IgGs were conjugated with NC-modified BSA. BSA functionalized Au/Pt NCs (Au/Pt NCs-BSA)

were synthesized following the same aforementioned method.³⁷ Then, the carboxyl groups of anti-rabbit IgGs (1000 $\mu\text{g mL}^{-1}$) were activated *via* carbodiimide chemistry by incubating with EDC (2 mM) and NHS (5 mM) for 15 minutes. Then, the solution was filtered using Amicon filters (30 kDa cutoff) at $10\,000 \times g$ for 15 min to eliminate the excess of EDC and NHS. Next, the previously synthesized Au/Pt NCs-BSA conjugates were added to the solution (molar ratio IgG/BSA = 1 : 3). After incubation for 1 h at RT, the solution was purified using Amicon filters (100 kDa cutoff) to separate the Au/Pt NCs-BSA from the bioconjugate (IgG@Au/Pt NCs-BSA).

2.4. Characterization of the metallic NCs

UV-visible measurements were performed on a Synergy H1 microplate reader (BioTek) controlled by BioTek Gen5 Software. Transmission electron microscopy (TEM) images were obtained using JEM-2100F [Model EM-20014, UHR, 200 kV] (JEOL, Japan) equipped with a digital camera of type F-216 (TVIPS, Germany). A tiny droplet of the freshly made solution was desiccated on the hydrophilized surface of a Cu grid coated with an ultrathin carbon layer to create the samples. X-Ray photoelectron spectroscopy (XPS) experiments were performed using a VersaProbe III Physical Electronics (ULVAC) spectrometer with a monochromatic X ray source (aluminium $\text{K}\alpha$ line of 1487 eV), calibrated using the $3d_{5/2}$ line of Ag at 368.26 eV. Samples were deposited and dried on ultraflat silicon wafer and mounted with no conductive tape. Z-alignment was performed for optimal sample height prior to each sample measurement. Elemental quantification was done on survey scan with step energy 0.5 eV, pass energy 224 eV, while high resolution regions

were acquired with a step energy of 0.1 eV, a pass energy of 112 eV, and a time per step of 50 ms. The calibration of the spectrum fixed C 1s sp³ at 284.8 eV. CasaXPS software (2.3.16 PR 1.6) was used to analyze the data.

2.5. Catalytic activity of Au/Pt NCs-IgG

The catalytic activity of Au/Pt NCs-IgG was evaluated in experiments conducted at RT using 96-well microplates. The peroxidase-like activity was measured using TMB as the chromogenic substrate in the presence of H₂O₂. Each reaction mixture (final volume of 100 μL) contained Au/Pt NCs-IgG in 10 mM citrate buffer (pH 4.0). The concentration of TMB and H₂O₂ affects the peroxidase-like activity of the NCs. The concentration of one substrate was fixed, while the concentration of the other was varied in order to quantify how the initial reaction rate depended on the concentration of both substrates. As the enzymatic reaction takes place and TMB is oxidized by the action of the NCs, a color change from colorless to blue is observed. The reaction was stopped after 10 minutes by adding HCl 1 M, and the absorbance was measured at 450 nm. Using the Lineweaver–Burk equation,⁴⁴

$$\frac{1}{v} = \frac{K_m}{V_{\max}} \cdot \frac{1}{[S]} + \frac{1}{V_{\max}} \quad (1)$$

The Michaelis–Menten constant (K_m) was determined, where v is the initial velocity, $[S]$ is the substrate concentration, and V_{\max} is the maximal response velocity. Enzyme affinity to substrates is indicated by K_m ; a lower K_m denotes a stronger affinity.

2.6. Binding assays involving microscale thermophoresis (MST)

MST assays were carried out to confirm that the antibodies retained affinity after their modification with NCs. First, the target anti-rabbit IgG was fluorescently labeled by utilizing the commercial RED-NHS second generation protein Labeling Kit (Nanotemper Technologies GmbH, Munich, Germany). The protein was labelled by preparing a solution of 130 mM sodium bicarbonate and 50 mM NaCl (pH 8.2) with a concentration of 2 μM. It was then treated with a ten-fold excess of the fluorescent dye for 30 minutes at room temperature without illumination. The kit's gel filtration column was used to remove any unreacted dye. The ratio of absorption at 280 and 650 nm was used to calculate the degree of labeling, which came out to be 0.375 (dye/protein). For the binding assay, different concentrations of unlabeled IgG or Au/Pt NCs-IgG were mixed with a fixed concentration of 30 nM of fluorescent anti-rabbit IgG in PBST (150 mM NaCl, 50 mM phosphate, pH 7.4, 0.025% Tween[®] 20). A Monolith NT.115 system (Nanotemper Technologies GmbH, Munich, Germany) with a 20% LED excitation power and 40% MST power was then used to evaluate the materials after they had been loaded into capillaries. The Nanotemper analysis software (MO. Affinity Analysis) was employed to perform the data analysis.

2.7. Accelerated stability assays

The stability of a reagent indicates its ability to maintain consistent performance over time without degradation. It relates to the performance of a product within a specified time. The stability of Au/Pt NCs-IgG and the natural enzyme HRP in

solution were studied at 4 °C for 1, 3 and 6 months in accelerated assays at 37 °C. The equivalence to real time was calculated using the standard guide for Accelerated Aging of Sterile Barrier Systems for Medical Devices (ASTM).⁴⁵ Using the Arrhenius equation with Q_{10} equal to 2 is a conservative mean of calculating the accelerated aging factor (AAF). Thus, the AAF is calculated by the following equation:

$$AAF = Q_{10}^{\left(\frac{T_{AA}-T_{RT}}{10}\right)} \quad (2)$$

where T_{AA} = accelerated aging temperature (°C). T_{RT} = ambient temperature (°C).

The intended (or required) shelf life is divided by the AAF to find the accelerated aging time (AAT) required to achieve equivalency to real time aging.

$$AAT = \text{desired (RT)}/AAF \quad (3)$$

The AAT carried out at 37 °C for simulating the storage at 4 °C for 1, 3 and 6 months is 3, 6 and 9 days, respectively.

2.8. Optimization of the precursor mixture for Au/Pt NCs-IgG synthesis

The synthesis conditions for Au/Pt NCs-IgG were optimized by testing different concentrations of precursors. These Au/Pt NCs-IgGs were then employed in a direct immunoassay with and without the analyte. Then, the signal-to-noise ratio (SNR) was calculated to identify the synthesis that provided the most efficient detection of the antigen. A Nunc Maxisorp 96-well plate was used for the immunoassay. The control wells did not contain the antigen, and PBS was added instead. In the sample wells, anti-IL-6 IgG from a rabbit (100 μL, 50 μg mL⁻¹) was immobilized and incubated (overnight (ON), 4 °C). Then the surface was blocked with 100 μL of casein blocking solution (2 h, RT). Next came the addition of Au/Pt NCs-IgG (100 μL, 33 μg mL⁻¹) (1 h, RT). Finally, the concentration of rabbit IgG was related to the ability of Au/Pt NCs-IgG to oxidize the chromogenic substrate TMB (500 μM) in the presence of H₂O₂ (500 mM). The reaction was stopped after 10 minutes by adding HCl (100 μL, 1 M), and the absorbance was measured at 450 nm. After each step, the wells were washed three times with PBST (100 μL). The signal-to-noise ratio (SNR) was calculated by dividing the absorbance value obtained from the samples with the antigen by the absorbance value obtained from the control samples for each tested synthesis.

2.9. Dot-blot assay using Au/Pt NCs-IgG

The paper-based immunoassays were carried out on a nitrocellulose membrane with a pore size of 0.22 μm. 2 μL of anti-IL-6 IgGs from a rabbit at different concentrations (5, 10, 25, 50, 100, 250, and 500 μg mL⁻¹) were manually drop-casted on the membrane. After drying (10 min, RT), the membrane was blocked with casein blocking solution (1 h, RT) with gently shaking to prevent non-specific adsorption to the membrane. After the incubation time, the membrane was washed with 2 mL of PBST 3 times. Then, 2 mL of Au/Pt NCs-IgG or the IgG@Au/Pt NCs-BSA bioconjugates at a concentration of

33 $\mu\text{g mL}^{-1}$ (referred to IgG concentration) were incubated (1 h, RT) by shaking and then rinsed three times with 2 mL of PBST to get rid of the unbound IgG. Finally, 1 mL of TMB liquid solution for membranes was added onto it. The blue dots appeared visible by the naked eye in few seconds, getting darker in the next minutes. Photos were obtained after 5 minutes by using a smartphone camera. The intensity of these dots provided the concentration information of IgG from the rabbit. The quantification of the spots' intensity was performed with ImageJ software.⁴⁶

3. Results and discussion

3.1. Synthesis and characterization

Bimetallic NCs composed of gold and platinum were synthesised within the structure of a polyclonal anti-rabbit IgG according to the method described in the Experimental section, where the metal salts approach the disulfide bridges due to the sulfur-noble metal affinity, followed by a reduction step to form the NCs.

The stabilization of Au/Pt NCs is influenced by specific regions of the antibody, as demonstrated by using different antibody fragments as scaffolds for NC synthesis in a previous work.³⁷ Only the antibody fragments containing the hinge region, rich in disulfide bonds, were capable of forming Au/Pt NCs. The formation of NCs in this area is explained by the strong affinity of thiol groups for gold and platinum. The affinity of thiol groups for metals is well-known and is employed for the stabilization of nanomaterials, utilizing biomolecules rich in these groups, such as glutathione,⁴⁷ or organic compounds with mercapto groups.⁴⁸ Furthermore, the previous characterization of the catalytic activity of NCs suggests that the presence of both metals is necessary to achieve a significant reduction of TMB in the presence of H_2O_2 .³⁷

The synthesis conditions were set up to obtain the best signal-to-noise ratio (SNR) in a direct immunoassay. For this, different concentrations of metallic precursors and reducing agents were tested (Table S1, ESI†). In Fig. S1 (ESI†), the control values represent the noise due to non-specific interactions in the direct immunoassay. The sample values represent the signal due to the presence of the antigen. For each synthesis, the SNR was calculated by dividing the absorbance value of the antigen-containing samples by the absorbance value of the control samples (Fig. S2, ESI†). This ratio determines how effectively the antigen is detected relative to the background noise from the controls. A higher SNR indicates a more efficient detection of the antigen and, in consequence, it points at the most efficient concentrations during the synthesis step. The highest SNR was obtained at a final concentration of 330 $\mu\text{g mL}^{-1}$ of anti-rabbit IgG, 25 μM of HAuCl_4 , 200 μM of K_2PtCl_4 and 0.5 mM of NaBH_4 (Synthesis 3). Thus, further experiments were carried out using conjugates obtained under these conditions.

TEM was employed to analyze the morphology and size of Au/Pt NCs-IgG. Fig. 2A shows the spherical shape of the NCs. Statistical analysis of 100 individual NCs revealed a representative size of 2.08 ± 0.34 nm (Fig. 2B).

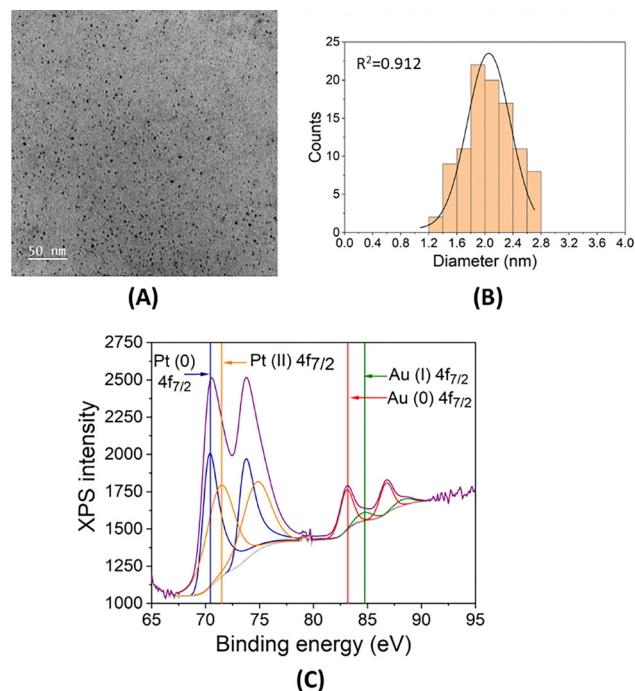


Fig. 2 (A) Representative TEM image. (B) Size distribution and XPS analysis of the Pt 4f and Au 4f spectra (C) of Au/Pt NCs-IgG.

XPS was employed to analyze the valence states of metallic NCs. The Pt 4f and Au 4f spectra of Au/Pt NCs-IgG are shown in Fig. 2C. The Pt 4f spectrum consists of two energy bands, the Pt 4f_{7/2} and the Pt 4f_{5/2} at 70.6 and 73.9 eV, respectively. This distribution of bands usually appears when Pt is in the metallic state. The Pt 4f_{7/2} spectrum was deconvoluted into two curves, an asymmetric Lorentzian curve for Pt(0) at 69.9 eV and a symmetric Gaussian-Lorentzian curve for Pt(II) at 71.4 eV. These peaks are typically found at 71 and 72.4 eV.⁴⁹ In the Au 4f region, the spectra display again two energy bands the 4f_{7/2} at 83.2 eV and the 4f_{5/2} at 86.8 eV. The Au 4f_{7/2} was fitted into two curves: one for Au(0) at 83.0 eV and another for Au(I) at 84.7 eV. Typically, these peaks are found at binding energies of 84 and 85 eV, respectively.⁵⁰ The variation between the standard values and those observed for the NCs indicates a significant interaction between Au and Pt atoms, resulting in the formation of Au-Pt alloys. This phenomenon has also been noted in other bimetallic NCs.⁵

3.2. Peroxidase-like activity of Au/Pt NCs-IgG

Au/Pt NCs-IgGs exhibit catalytic properties and can mimic the natural activity of the enzyme HRP, which catalyzes the oxidation of some substrates in the presence of H_2O_2 .⁵¹ This nanozyme behavior has already been observed in other nanomaterials such as gold nanomaterials,^{52,53} iron oxide nanoparticles,^{54,55} graphene,⁵⁶ and other hybrid metallic nanomaterials.⁵⁷⁻⁵⁹ Using the chromogenic substrate TMB, the peroxidase-like activity of Au/Pt NCs-IgG was analysed. TMB and H_2O_2 concentrations affect Au/Pt NCs-IgG's catalytic activity. The peroxidase-like activity of the NCs was measured in acetate buffer (10 mM, pH 4) by varying the concentration of one of the substrates while

keeping the other constant. To study the effect of TMB concentration on enzymatic activity, a range from 0 to 500 μM was tested with the concentration of H_2O_2 maintained at 500 mM. Similarly, when examining the effect of H_2O_2 concentration, a range from 0 to 500 mM was tested with the TMB concentration fixed at 500 μM . Fig. 3A and B show that in both cases, the absorbance at 450 nm increases with substrate concentration and furthermore, the curves fit a Michaelis–Menten model. The K_m toward TMB and H_2O_2 was calculated using the Lineweaver–Burk equation.⁴⁴ This constant indicates the affinity of an enzyme/nanozyme for its substrate, with a lower value indicating higher affinity. A K_m value of 15.080 mM towards H_2O_2 and a K_m value of 0.115 mM towards TMB were obtained for the Au/Pt NCs–IgG. Comparing these values with those of HRP found in studies performed under similar conditions⁵ (0.362 mM for TMB and 0.522 mM for H_2O_2), it is observed that Au/Pt NCs–IgG has 3.15 times greater affinity for TMB, but 28.9 times lower affinity for H_2O_2 than HRP. The higher affinity of HRP for H_2O_2 is attributed to the optimized active center with a specific heme group,⁶⁰ facilitating efficient substrate binding and catalysis.³⁹ This behavior has been observed in other nanozymes^{8,61} with highly variable K_m values, as summarized in Table 1. The Michaelis–Menten constant of our nanocluster falls within the range reported in the literature.

3.3. Binding assays by MST

To evaluate the impact of NC modification on antibody–antigen binding affinity, association assays were performed using MST to determine the dissociation constants (K_D) for both the naked antibody and the NC-modified antibody. The K_D of an antibody–antigen interaction quantifies the affinity between the

two molecules. A lower K_D value indicates a stronger binding affinity, while a higher K_D suggests weaker binding.⁷¹ As shown in Fig. 3C, the fraction bound *versus* antigen concentration curves for both the naked IgG and the Au/Pt NCs IgG illustrate comparable binding activity.

The naked antibody exhibited a K_D of 208.5 nM, while the NC-modified antibody showed a K_D of 204.5 nM. These highly similar values indicate that the modification of the antibody with NCs does not significantly affect its binding affinity for the antigen. In addition, the NCs do not interfere with the recognition site of the antibody. This indicates that the NCs do not form at or near the biorecognition site, thereby preserving the functional integrity of the antibody and antigen-binding capacity, reinforcing the conclusion that NC modification does not modify antigen binding. The preservation of binding affinity also implies that the global structure of the antibody remains largely intact following NC modification, indicating that the NCs do not induce significant conformational changes or denaturation.

3.4. Accelerated stability assay

Natural enzymes, while highly efficient and specific in catalyzing biochemical reactions, are often sensitive to environmental changes. This sensitivity can lead to a loss of activity over time, limiting their practical applications in various industries.⁷² Nanomaterials, on the other hand, exhibit improved stability and are less prone to denaturation under harsh conditions maintaining their catalytic activity over extended periods and a wider range of environments.⁷³ The stability of Au/Pt NCs–IgG and the natural enzyme HRP in solution was compared through accelerated stability assays at 37 °C, simulating storage at 4 °C for 1, 3, and 6 months. Fig. 3D shows the percentage of catalytic activity maintained over time (1, 3, and 6 months), with 100% representing the catalytic activity obtained with fresh reagents.

It is observed that in solution, the natural enzyme HRP loses almost all its activity after 1 month of storage. However, the Au/Pt NCs–IgGs retain 97% of their activity in solution after 1 month, 80% after 3 months, and more than 70% after 6 months. These results demonstrate the superior stability of the NCs for long-term storage in solution compared to the natural enzyme HRP.

Despite the initial high catalytic activity of HRP, it rapidly denatures and loses functionality, making it less viable for applications requiring prolonged storage. In contrast, the Au/Pt NCs–IgGs not only exhibit a high initial catalytic activity but also maintain a significant portion of this activity over extended periods. This enhanced stability can be attributed to the robust nature of the nanomaterials, which are less susceptible to environmental changes and degradation. Thus, the Au/Pt NCs–IgGs present a more reliable and durable option for applications where long-term stability is crucial. This phenomenon has already been observed in other nanomaterials, such as hybrid nanoparticles.⁷⁴

3.5. Dot-blot immunoassays

The paper-based immunoassay for detecting IgG from a rabbit employed Au/Pt NCs–IgG as the detection and transduction

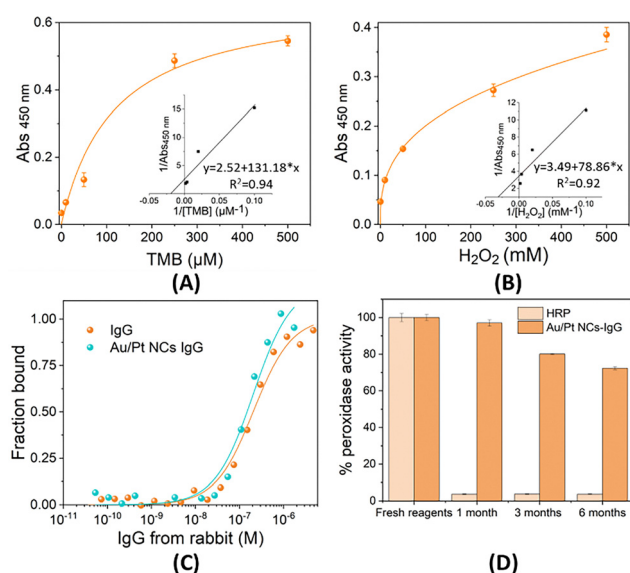


Fig. 3 (A) and (B) intensity of the absorbance peak (450 nm) and Lineweaver–Burk plots at different TMB and H_2O_2 concentrations catalyzed by Au/Pt NCs–IgG. (C) Binding affinity curves for naked IgG and Au/Pt NCs–IgG. (D) Normalized peroxidase activity for HRP and Au/Pt NCs–IgG in solution for fresh reagents and after storage for 1, 3 and 6 months at 4 °C (accelerated assays performed at 37 °C).

Table 1 Examples of protein-protected NCs with enzyme-like activity and their applications

NCs	Protective biomolecule	Catalytic type	Catalytic activity	Application
AuNCs ⁶²	BSA	Peroxidase	H ₂ O ₂ <i>K_M</i> : 25.3 mM TMB <i>K_M</i> : 0.00253 mM	Colorimetric detection of H ₂ O ₂ (LOD: 2×10^{-8} M) and xanthine (LOD: 5×10^{-7} M)
AuNCs ⁶³	BSA	Peroxidase	H ₂ O ₂ <i>K_M</i> : 2.46 mM TMB <i>K_M</i> : 0.00664 mM	Tumor molecular location and diagnosis
AuNCs ⁶⁴	Apoferitin	Peroxidase	H ₂ O ₂ <i>K_M</i> : 199.4 mM TMB <i>K_M</i> : 0.097 mM	Colorimetric detection of glucose
AuNCs ⁶⁵	Protamine	Peroxidase	H ₂ O ₂ <i>K_M</i> : 1.49 mM TMB <i>K_M</i> : 0.169 mM	Colorimetric detection of Hg ²⁺ (LOD: 1.16 nM)
PtNCs ⁶⁶	BSA	Peroxidase	H ₂ O ₂ <i>K_M</i> : 41.8 mM TMB <i>K_M</i> : 0.119 mM	Colorimetric detection of Hg ²⁺ (LOD: 7.2 nM)
CuNCs ⁶⁷	BSA	Peroxidase	H ₂ O ₂ <i>K_M</i> : 0.0089 mM TMB <i>K_M</i> : 0.00138 mM	Colorimetric detection of xanthine (LOD: 3.8×10^{-7} M)
AgNCs ⁶⁸	BSA	Oxidase	—	Colorimetric immunoassay for <i>Listeria monocytogenes</i> (LOD: 10 cfu mL ⁻¹)
PtNCs ⁶⁹	Lysozyme	Oxidase	TMB <i>K_M</i> : 0.63 mM	Degradation of methylene blue in the absence of H ₂ O ₂
PtNCs ⁷⁰	Ferritin	Catalase	H ₂ O ₂ <i>K_M</i> : 420.6 mM	—

element. The signal was generated taking advantage of the catalytic properties of the NCs towards TMB oxidation in the presence of H₂O₂. The complete detection procedure including the synthesis of the bimetallic NCs is illustrated in Fig. 1B.

The dot-blot immunoassay was performed as described in the Experimental section. First, the antigen (IgG from a rabbit) was drop-casted in the nitrocellulose membrane, followed by a blocking step. Au/Pt NCs-IgGs were then added, and after incubation time, finally the insoluble TMB formed a precipitate easily seen by the naked eye. Fig. 4A shows an image of the nitrocellulose membrane after the reaction. The concentration of rabbit IgG causes the spots to become more intense. Fig. 4C provides the profile graphs.

We studied the performance of our system compared to a similar probe that employs IgG bioconjugation to couple NCs embedded in the structure of BSA. Here, NCs were synthesized following the same procedure as for Au/Pt NCs-IgG but embedded within the BSA structure, which also presents disulfide structures. Subsequently, NCs-BSA were coupled to anti-rabbit IgG using EDC/NHS coupling. These bioconjugates were characterized by TEM and XPS to confirm properties similar to those of NCs stabilized in IgG (see Fig. S3 and S4, ESI†).

This bioconjugate was used as the detection antibody in a dot-blot immunoassay, repeating the conditions used for Au/Pt NCs-IgG. Fig. 4B shows an increase in spot intensity with antigen concentration. Analysis of spot intensities from each lane can be found in Fig. 4D.

In Fig. 5A, the biosensing responses for both conjugates are compared. The limit of detection (LOD) was calculated as three times the standard deviation of the blank divided by the slope of the calibration curve. Both methods exhibited very low non-specific adsorption, although Au/Pt NCs-IgG achieved a LOD three times better (200 ng mL⁻¹) than IgG@Au/Pt NCs-BSA bioconjugates (660 ng mL⁻¹).

Furthermore, the specificity was confirmed by repeating the immunoassay using IgG from sheep as the antigen instead of an IgG from a rabbit, observing no visible signal (Fig. 5B).

Integrating NCs within the antibody structure allows for precise control over their spatial orientation relative to the

antigen-binding site. This alignment can optimize the interaction between IgG-NCs and target antigens, potentially increasing the efficiency of antigen recognition and binding. In contrast, coupling *via* EDC/NHS could result in some NCs-BSA positioning in the binding region, thereby decreasing biorecognition efficiency.⁷⁵ Moreover, the bioconjugate could induce steric hindrance within the antigen-antibody complex. By integrating NCs directly into the antibody structure, steric hindrance can be minimized, allowing for better accessibility of the antigen-binding site and potentially enhancing sensitivity.

To explore the applicability of the developed immunoassay in more complex biological environments, the dot-blot assay was performed using serum as the sample matrix instead of buffer. The experimental conditions were maintained identical to those described previously. As shown in Fig. 5C, a higher level of non-specific adsorption was observed when using serum, as indicated by the signal corresponding to the blank sample (0 µg mL⁻¹), which consisted of serum alone without the target antibody.

Despite the increased background, a visible and concentration-dependent signal was still obtained. The calibration curve obtained in serum, shown in purple in Fig. 5A, was constructed by subtracting the background signal corresponding to the blank. The LOD was 552 ng mL⁻¹, reflecting the greater complexity and interference inherent to serum samples. Nonetheless, these results demonstrate that the immunoassay retains good sensitivity even in the presence of complex biological matrices, reinforcing its potential for direct application to clinical samples.

4. Conclusions

In this study, a dot-blot immunoassay based on Au/Pt bimetallic nanoclusters (NCs) embedded in anti-rabbit IgG was developed for the detection of anti-IL6 IgG produced in rabbits. The modified antibody can mimic the behavior of the natural enzyme HRP and is capable of oxidizing chromogenic substrates, such as TMB, in the presence of H₂O₂. This property has been utilized for the development of a paper-based

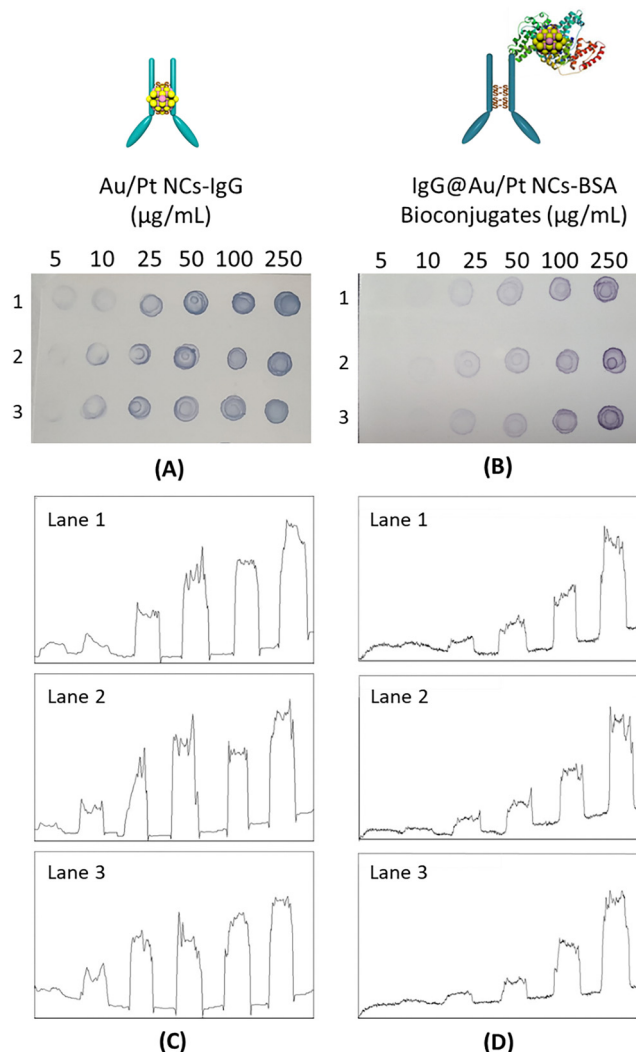


Fig. 4 (A) and (B) Dot-blot immunoassay and (C) and (D) intensity measurement of the resulting spots employing Au/Pt NCs-IgG and IgG@Au/Pt NCs-BSA bioconjugates as detection antibodies.

immunoassay. In the dot-blot assay, Au/Pt NCs-IgG serves as a probe, incorporating both the detection and transduction elements. The catalytic properties of the NCs towards TMB oxidation generate a signal proportional to the antigen concentration, which can be observed by the naked eye and quantified after simple processing. Additionally, Au/Pt NCs-IgG demonstrated superior stability in solution compared to the natural enzyme HRP. Furthermore, the performance of Au/Pt NCs-IgG was compared with a bioconjugate where the BSA-stabilized Au/Pt NCs were linked to the antibody *via* EDC/NHS. The immunoassay using Au/Pt NCs-IgG exhibited greater sensitivity than the bioconjugate. This new method offers the potential to develop biosensors that do not require complex labeling, possess excellent catalytic properties, and are suitable for lab-on-a-chip (LoC) applications due to their ability to retain properties over extended periods. Moreover, the assay maintained a detectable and quantifiable signal when anti-IL-6 IgG from the rabbit was dissolved in human serum despite the increased

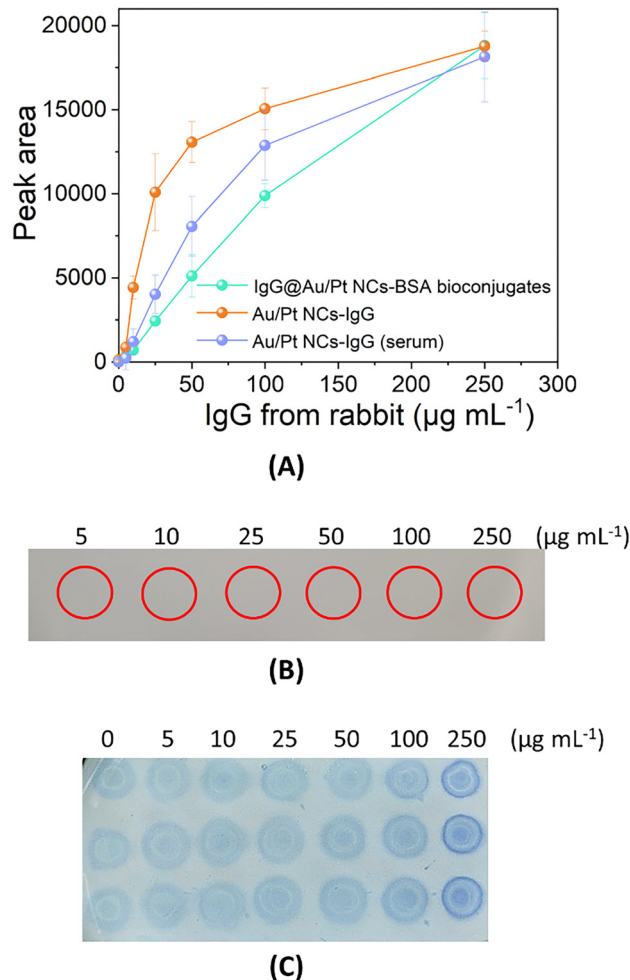


Fig. 5 (A) Corresponding peak areas obtained from profile plots employing Au/Pt NCs-IgG and IgG@Au/Pt NCs-BSA. (B) Control dot-blot immunoassay for IgG from sheep quantification employing Au/Pt NCs-IgG as the detection antibody. The red circumferences indicate the spot of drop-casted sheep IgG. (C) Dot-blot immunoassay carried out in human serum.

complexity of the matrix. These results further support the robustness and versatility of the platform for potential clinical sample analysis.

Author contributions

Verónica Mora-Sanz: methodology, visualization, investigation and writing – original draft. Laura Saa: methodology, investigation and writing – original draft. Valeri Pavlov: conceptualization. Aitziber L. Cortajarena: funding acquisition and writing – review and editing. Bergoi Ibarlucea: supervision and writing – review and editing. Nerea Briz: conceptualization, funding acquisition, supervision and writing – review and editing.

Data availability

All relevant data are available from the authors on reasonable request and/or are included within the article and the ESI.†

Conflicts of interest

There are no conflicts to declare.

Acknowledgements

This work was supported by the European Union's 2020 research and innovation FET Open program under grant agreement 964248 (DeDNAed project). A. L. C. acknowledges the support by the Agencia Estatal de Investigación, grants PDC2021-120957-I00 (NanoIVDab) and PID2022-137977OB-I00 (ProTHER) funded by MCIN/AEI/10.13039/501100011033 and by the "European Union NextGenerationEU/PRTR". This work was performed under the Maria de Maeztu Units of Excellence Program from the Spanish State Research Agency – Grant No. MDM-2017-0720.

Notes and references

- P. V. Surti, M. W. Kim, L. M. T. Phan, S. K. Kailasa, A. K. Mungray, J. P. Park and T. J. Park, *TrAC, Trends Anal. Chem.*, 2022, **157**, 116736.
- K. E. Sapsford, L. Berti and I. L. Medintz, *Angew. Chem., Int. Ed.*, 2006, **45**, 4562–4589.
- T. L. Rocha, N. C. Mestre, S. M. T. Sabóia-Morais and M. J. Bebianno, *Environ. Int.*, 2016, **98**, 1–17.
- S. Krishnan and Z. ul Q. Syed, *Sens. Actuators Rep.*, 2022, **4**, 100078.
- J. Feng, P. Huang and F. Wu, *Analyst*, 2017, **142**, 4106–4115.
- J. Wu, X. Wang, Q. Wang, Z. Lou, S. Li, Y. Zhu, L. Qin and H. Wei, *Chem. Soc. Rev.*, 2019, **48**, 1004.
- V. Sharma and M. Bachwani, *Curr. Enzyme Inhib.*, 2011, **7**, 178–189.
- L. Gao, J. Zhuang, L. Nie, J. Zhang, Y. Zhang, N. Gu, T. Wang, J. Feng, D. Yang, S. Perrett and X. Yan, *Nat. Nanotechnol.*, 2007, **2**, 577–583.
- M. Zandieh and J. Liu, *Adv. Mater.*, 2024, **36**, 2211041.
- R. Zhang, K. Fan and X. Yan, *Sci. China: Life Sci.*, 2020, **63**, 1183–1200.
- H. Wei, H. Huang, H. He, Y. Xiao, L. Chun, Z. Jin, H. Li, L. Zheng, J. Zhao and Z. Qin, *Research*, 2024, **7**, 0310.
- L. Ding, L. Wang, J. Zhang, N. Ren, A. Wang, H. Liu and X. Yu, *Adv. Powder Mater.*, 2024, **3**, 100191.
- X. Xu, L. Wang, X. Zou, S. Wu, J. Pan, X. Li and X. Niu, *Sens. Actuators, B*, 2019, **298**, 126876.
- S. Hu, Y. Jiang, Y. Wu, X. Guo, Y. Ying, Y. Wen and H. Yang, *ACS Appl. Mater. Interfaces*, 2020, **12**, 55324–55330.
- Q. Yang, L. Li, F. Zhao, Y. Wang, Z. Ye and X. Guo, *Mater. Lett.*, 2019, **248**, 89–92.
- J. Xie, M. Q. Tang, J. Chen, Y. H. Zhu, C. B. Lei, H. W. He and X. H. Xu, *Talanta*, 2020, **217**, 121070.
- N. Cheng, Y. Song, M. M. A. Zeinhom, Y. C. Chang, L. Sheng, H. Li, D. Du, L. Li, M. J. Zhu, Y. Luo, W. Xu and Y. Lin, *ACS Appl. Mater. Interfaces*, 2017, **9**, 40671–40680.
- D. Duan, K. Fan, D. Zhang, S. Tan, M. Liang, Y. Liu, J. Zhang, P. Zhang, W. Liu, X. Qiu, G. P. Kobinger, G. Fu Gao and X. Yan, *Biosens. Bioelectron.*, 2015, **74**, 134–141.
- X. Lai, G. Zhang, L. Zeng, X. Xiao, J. Peng, P. Guo, W. Zhang and W. Lai, *ACS Appl. Mater. Interfaces*, 2021, **13**, 1413–1423.
- L.-Y. Chen, C.-W. Wang, Z. Yuan and H.-T. Chang, *Anal. Chem.*, 2015, **87**, 216–229.
- X. Le Guével, *IEEE J. Sel. Top. Quantum Electron.*, 2014, **20**(3), 45–56.
- S. Guo and E. Wang, *Nano Today*, 2011, 240–264.
- D. Jariwala, V. K. Sangwan, L. J. Lauhon, T. J. Marks and M. C. Hersam, *Chem. Soc. Rev.*, 2013, **42**, 2824.
- T. Ishida, T. Murayama, A. Taketoshi and M. Haruta, *Chem. Rev.*, 2020, **120**, 464–525.
- G. L. Wang, L. Y. Jin, Y. M. Dong, X. M. Wu and Z. J. Li, *Biosens. Bioelectron.*, 2015, **64**, 523–529.
- H. W. Li, Y. Yue, T. Y. Liu, D. Li and Y. Wu, *J. Phys. Chem. C*, 2013, **117**, 16159–16165.
- N. Pajoohepour, M. Rezaei, A. Hajian, A. Afkhami, M. Sillanpää, F. Arduini and H. Bagheri, *Sens. Actuators, B*, 2018, **275**, 180–189.
- H. Kawasaki, K. Hamaguchi, I. Osaka and R. Arakawa, *Adv. Funct. Mater.*, 2011, **21**, 3508–3515.
- Y. Xu, J. Sherwood, Y. Qin, D. Crowley, M. Bonizzoni and Y. Bao, *Nanoscale*, 2014, **6**, 1515–1524.
- H. Miao, D. Zhong, Z. Zhou and X. Yang, *Nanoscale*, 2015, **7**, 19066–19072.
- Y. Noh, E. J. Jo, H. Mun, Y. deok Ahn and M. G. Kim, *Chemosphere*, 2017, **174**, 524–530.
- A. L. Cortajarena, A. Aires, A. Sousaraei, M. Möller and J. Cabanillas-Gonzalez, *Nano Lett.*, 2021, **21**, 9347–9353.
- A. Aires, I. Llarena, M. Moller, J. Castro-Smirnov, J. Cabanillas-Gonzalez and A. L. Cortajarena, *Angew. Chem., Int. Ed.*, 2019, **58**, 6214–6219.
- E. Lopez-Martinez, D. Gianolio, S. Garcia-Orrit, V. Vega-Mayoral, J. Cabanillas-Gonzalez, C. Sanchez-Cano and A. L. Cortajarena, *Adv. Opt. Mater.*, 2022, **10**, 2101332.
- A. Aires, D. Maestro, J. Ruiz del Rio, A. R. Palanca, E. Lopez-Martinez, I. Llarena, K. Geraki, C. Sanchez-Cano, A. V. Villar and A. L. Cortajarena, *Chem. Sci.*, 2021, **12**, 2480–2487.
- P. Couleaud, S. Adan-Bermudez, A. Aires, S. H. Mejias, B. Sot, A. Somoza and A. L. Cortajarena, *Biomacromolecules*, 2015, **16**, 3836–3844.
- V. Mora-Sanz, L. Saa, N. Briz and V. Pavlov, *Chem. Mater.*, 2020, **32**, 8286–8293.
- V. Mora-Sanz, L. Saa, N. Briz, M. Möller and V. Pavlov, *ACS Appl. Mater. Interfaces*, 2020, **12**, 28993–28999.
- R. López-Domene, S. Vázquez-Díaz, E. Modin, A. Beloqui and A. L. Cortajarena, *Adv. Funct. Mater.*, 2023, **33**, 2301131.
- T. Hirano, *Proc. Jpn. Acad., Ser. B*, 2010, **86**, 717–730.
- X. Wang, J. Li, W. Liu, X. Zhang and L. Xue, *Medicine*, 2021, **100**(47), e27945.
- A. Santa Cruz, A. Mendes-Frias, A. I. Oliveira, L. Dias, A. R. Matos, A. Carvalho, C. Capela, J. Pedrosa, A. G. Castro and R. Silvestre, *Front. Immunol.*, 2021, **12**, 613422.
- B. Liang, D. B. Gardner, D. E. Griswold, P. J. Bugelski and X. Y. R. Song, *Immunology*, 2006, **119**, 296–305.
- H. Lineweaver and D. Burk, *JACS*, 1934, **56**, 658–666.

- 45 ASTM International, F1980-07. Standard Guide for Accelerated Aging of Sterile Barrier Systems for Medical Devices, 2007.
- 46 A. Nagarajan, R. Janostiak and N. Wajapeyee, *Methods Mol. Biol.*, 2019, **1870**, 263–271.
- 47 J. G. You and W. L. Tseng, *Anal. Chem.*, 2019, **1078**, 101–111.
- 48 M. Cargnello, N. L. Wieder, P. Canton, T. Montini, G. Giambastiani, A. Benedetti, R. J. Gorte and P. Fornasiero, *Chem. Mater.*, 2011, **23**, 3961–3969.
- 49 J. Zeng, J. Yang, J. Y. Lee and W. Zhou, *J. Phys. Chem. B*, 2006, 24606–24611.
- 50 M. P. Casaletto, A. Longo, A. Martorana, A. Prestianni and A. M. Venezia, *Surf. Interface Anal.*, 2006, **38**, 215–218.
- 51 N. C. Veitch, *Phytochemistry*, 2004, **65**, 249–259.
- 52 L. Wu, M. Zhang, L. Zhu, J. Li, Z. Li and W. Xie, *Microchem. J.*, 2020, **157**, 105079.
- 53 L. Jiao, W. Xu, H. Yan, Y. Wu, W. Gu, H. Li, D. Du, Y. Lin and C. Zhu, *Chem. Commun.*, 2019, **55**, 9865–9868.
- 54 W. Li, G. C. Fan, F. Gao, Y. Cui, W. Wang and X. Luo, *Biosens. Bioelectron.*, 2019, **127**, 64–71.
- 55 P. Šálek, A. Golunova, J. Dvořáková, E. Pavlova, H. Macková and V. Proks, *Mater. Lett.*, 2020, **269**, 1–4.
- 56 A.-X. Zheng, Z.-X. Cong, J.-R. Wang, J. Li, H.-H. Yang and G.-N. Chen, *Biosens. Bioelectron.*, 2013, **49**, 519–524.
- 57 F. Wang, Y. Zhang, Z. Liu, J. Ren and X. Qu, *Nanoscale*, 2020, **12**, 14465–14471.
- 58 M. Mirhosseini, A. Shekari-Far, F. Hakimian, B. F. Haghiralsadat, S. K. Fatemi and F. Dashtestani, *Process Biochem.*, 2020, **95**, 131–138.
- 59 Y. Wang, H. Li, L. Guo, Q. Jiang and F. Liu, *RSC Adv.*, 2019, **9**, 18815.
- 60 R. W. Noble and Q. H. Gibson, *J. Biol. Chem.*, 1970, **245**, 2409–2413.
- 61 Q. Xian-ming, Z. Liu, S. Cai, Y. Zhao and D. Wu, *Chin. Chem. Lett.*, 2016, 1–7.
- 62 X. Wang, Q. Wu, Z. Shan and Q. Huang, *Biosens. Bioelectron.*, 2011, **26**, 3614–3619.
- 63 D. Hu, Z. Sheng, S. Fang, Y. Wang, D. Gao, P. Zhang, P. Gong, Y. Ma and L. Cai, *Theranostics*, 2014, **4**, 142–153.
- 64 X. Jiang, C. Sun, Y. Guo, G. Nie and L. Xu, *Biosens. Bioelectron.*, 2015, **64**, 165–170.
- 65 Y. Q. Huang, S. Fu, Y. S. Wang, J. H. Xue, X. L. Xiao, S. H. Chen and B. Zhou, *Anal. Bioanal. Chem.*, 2018, **410**, 7385–7394.
- 66 W. Li, B. Chen, H. Zhang, Y. Sun, J. Wang, J. Zhang and Y. Fu, *Biosens. Bioelectron.*, 2015, **66**, 251–258.
- 67 Z. Yan, Q. Niu, M. Mou, Y. Wu, X. Liu and S. Liao, *J. Nanopart. Res.*, 2017, **19**, 235.
- 68 Y. Liu, J. Wang, X. Song, K. Xu, H. Chen, C. Zhao and J. Li, *Microchim. Acta*, 2018, **185**, 2–8.
- 69 C. J. Yu, T. H. Chen, J. Y. Jiang and W. L. Tseng, *Nanoscale*, 2014, **6**, 9618–9624.
- 70 J. Fan, J. Yin, B. Ning, X. Wu, Y. Hu, M. Ferrari, G. J. Anderson, J. Wei, Y. Zhao and G. Nie, *Biomater.*, 2011, **32**, 1611–1618.
- 71 D. Breitsprecher, B. Kern, A. Gupta, I. Bekic and N. Tschammer, *J. Proteins Proteomics*, 2018, **9**, 73–76.
- 72 S. Li, X. Yang, S. Yang, M. Zhu and X. Wang, *Comput. Struct. Biotechnol. J.*, 2012, **2**, e201209017.
- 73 H. Wei and E. Wang, *Chem. Soc. Rev.*, 2013, **42**, 6060–6093.
- 74 P. Wu, P. Ding, X. Ye, L. Li, X. He and K. Wang, *RSC Adv.*, 2019, **9**, 14982–14989.
- 75 R. Raghav and S. Srivastava, *Biosens. Bioelectron.*, 2016, **78**, 396–403.